ACS APPLIED MATERIALS & INTERFACES

Research Article

www.acsami.org

Self-Assembled Reduced Graphene Oxide/Polyacrylamide Conductive Composite Films

Shiyou Yu,[†] Ning Li,*[,†] Drew Higgins,[‡] Deyu Li,[†] Qing Li,[‡] Hui Xu,[‡] Jacob S. Spendelow,[‡] and Gang Wu*[,§]

[†]School of Chemical Engineering & Technology, Harbin Institute of Technology, Harbin, 150001, China

[‡]Materials Physics and Applications Division, Los Alamos National Laboratory, Los Alamos, New Mexico 87545, United States

[§]Department of Chemical and Biological Engineering, University at Buffalo, The State University of New York, Buffalo, New York 14260, United States

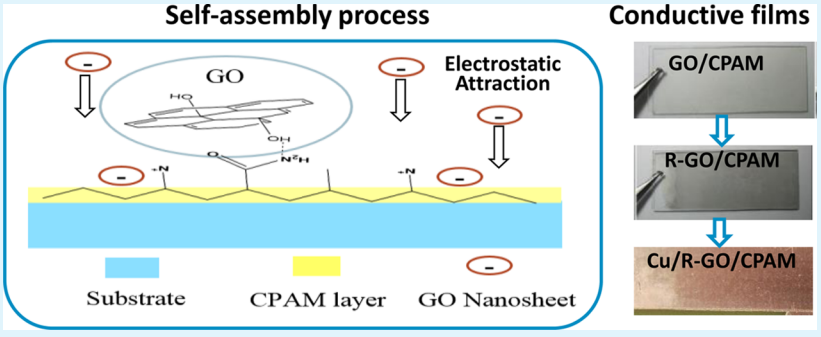

ABSTRACT: Substrate supported conductive thin films are prepared by the self-assembly of graphene oxide (GO) on a cationic polyacrylamide (CPAM) layer followed by a subsequent chemical reduction. During self-assembly, the dispersed GO nanosheets with a negative zeta potential from solution are spontaneously assembled onto the positively charged CPAM adsorption layer. In addition, CPAM adsorption on the substrate is studied with an electrochemical quartz crystal microbalance (EQCM), showing adsorption stabilization could be established in less than 150 s. The electrostatic interactions between GO and CPAM are investigated by changing the polarization potential with EQCM for the first time, and optimal conditions for facilitating self-assembly are determined. The self-assembled GO/CPAM films are further characterized by Raman spectroscopy, infrared spectroscopy and atomic force microscopy. Importantly, reduced GO (R-GO)/CPAM composite films exhibiting a sheet resistance of 3.1 kΩ/sq can be obtained via in situ reduction in sodium borohydride for 20 min at room temperature. This provides a simple, highly effective, and green route to prepare conductive graphene-based composite thin films.

KEYWORDS: *self-assembly, graphene oxides, reduced graphene oxides, polyacrylamide, conductive films, copper electrodeposition*

1. INTRODUCTION

Since its discovery, graphene has been gaining increasing attention for both fundamental and applied materials research.[1] Theoretically, graphene is a two-dimensional (2D) monolayer with a thickness of 0.34 nm,[2] and shows unique structural, thermal and electrical properties,[1] including the quantum Hall effect at room temperature and an electron mobility in excess of 250 000 $cm^2/V{\cdot}s$.[3,4] Several reliable methods have been developed for graphene preparation, including chemical vapor deposition,[5,6] graphite exfoliation,[7−9] epitaxial growth,[10−13] polymer graphitization,[14−16] and reduction of graphene oxide (GO).[17−20] This has opened up new opportunities to prepare graphene-based conductive films,[19,21−24] which have generally relied on the preparation of graphene by GO reduction.[22,25−28] These graphene-based conductive films usually comprise graphene and organic components,[29,30] such as electrically conducting polymers,[31−33] to prepare composite structures with high binding strength, electrical conductivity, and high flexibility.[34] However, high contact resistances caused by agglomeration or poor interconnectivity of the graphene nanosheets within the film still need to be overcome. Therefore, to overcome the shortcomings, self-assembly methods have been used to fabricate graphene-based conductive films.

Layer-by-layer assembled GO/polymer composite films were first proposed by Kotov et al.,[35,36] whereby it was reported that GO nanosheets could be assembled onto substrates treated with cationic surfactants. Because of the weak adsorption of GO nanosheets on the cationic poly(diallyl dimethyl) ammonium chloride pretreatment surfactant, successive deposition of 25 alternating layers was required to ensure sufficient film thicknesses and avoid ultrahigh film resistance values. This GO composite film was then hydrazine-treated and subsequently annealed at 400 °C for 1 h to transform the thin film

Received: July 28, 2014
Accepted: October 20, 2014
Published: October 20, 2014

from an insulator to a conductor.[37] While successful in terms of material preparation, this complex and time-consuming process relies on a toxic reducing agent, rendering it unsuitable for large scale industrial production. On the other hand, sodium borohydride has been demonstrated as a more effective reduction reagent than hydrazine hydrate for GO.[27] Unfortunately, during the rapid sodium borohydride induced reduction process, the evolution of hydrogen bubbles can lead to detachment of the GO film from the underlying substrate, or deterioration of the overall structure into small graphene debris.[19] Therefore, proper selection and processing of the surfactant pretreatment layer is necessary to facilitate the successful self-assembly of GO nanosheets, and to strengthen the binding force between the GO film and the substrate.

The discovery of more effective surfactant pretreatment species with strengthened interactions, and thus a single-step deposition process to efficiently form GO film, is highly desirable. Our work was inspired by the use of polyacrylamide in the dyeing industry, municipal wastewater treatment and paper printing.[38] This polyacrylamide molecule possesses reactive species that render it highly effective as a flocculating agent for these applications. As GO nanosheets possess a high concentration of oxygen-containing functional groups, they generally have a negative ζ potential in solutions. Thererefore, cationic polyacrylamide (CPAM) was selected as the intermediate pretreatment layer in this study as it can provide favorable electrostatic interactions. More importantly, because CPAM can conglutinate on substrate surfaces rapidly with a strong adsorption capacity, it provides unique synthetic capabilities that include the preparation of self-assembled GO/CPAM bilayer films. Subsequently, the composite film was reduced at room temperature using sodium borohydride solution, forming a R-GO/CPAM conductive layer. This facile, timely, and efficient approach has never been reported before, and we investigate and report on the unique driving and binding forces occurring during the self-assembly process. Moreover, a patterned copper coating is deposited uniformly on these unique conductive films, demonstrating the great application potential in the field of electronics.

2. EXPERIMENTAL SECTION

2.1. Preparation of Graphite Oxide Dispersion and Pretreatment Solution. GO was synthesized from natural graphite powder (350 mesh, Jasen Graphite, China) by the Hummers method.[39] The exfoliation of GO nanosheets was achieved by ultrasonication for 40 min, and the product was filtered and washed with 5 vol % hydrochloric acid three times to remove metal ions. GO dispersion was achieved with a concentration of 0.1 mg/mL by adding DI water, and the pH value was adjusted by the addition of KOH.

CPAM (a copolymer of acrylamide and acryloyloxyethyl trimethylammonium chloride from SNF Group) was used to prepare the pretreatment solution. Specified concentrations of various CPAM particles were slowly added into DI water with rapid stirring at 50 °C and continued stirring until the solution turned viscous, transparent and no fine particles were observed. Finally, the mixture was adjusted to pH 7.0 by the addition of KOH and stirred for 24 h at room temperature.

2.2. Self-Assembled Deposition of GO/CPAM Composite Films. All substrates including glass slides, epoxy plastic plates, copper sheets and silicon wafers were degreased and cleaned. First, the samples were sonicated in ethanol for 10 min and rinsed in DI water twice. In the case of copper sheets, they were immersed in 5 vol % hydrochloric acid to remove the oxide films. No surface roughening processes were employed throughout these experiments.

GO/CPAM composite films were prepared on the substrate surface by the deposition of CPAM as an initial adsorption layer, followed by the deposition of GO nanosheets with an opposite charge. Initially, the samples were immersed in the pretreatment solution for various time periods as outlined in the Results and Discussion section. After they were rinsed with DI water and careful drying with a cold air dryer, the CPAM coated substrates were immersed into the GO dispersion (0.1 mg/mL) for 10 min. GO nanosheets self-assembled on the CPAM layer during the immersion process. The film coated substrates were rinsed once again with DI water to remove any weakly bound GO.

2.3. Reduction of GO/CPAM Composite Films with Sodium Borohydride. A fresh aqueous solution of sodium borohydride was prepared with a concentration of 1.0 mg/mL as the reducing solution. The substrates with GO/CPAM composite films were then immersed in the reducing solution for 20 min at room temperature.

2.4. Characterization of Self-Assembled Composite Films. Contact angle measurements were carried out using a Dataphysics OCA20 contact angle system at room temperature. ζ potentials of the GO dispersions were measured using a particle size analyzer (Zetasizer Nano ZSP) at room temperature. The morphology of the GO films were examined by field-emission scanning electron microscopy (Quanta 200FEG). The films of GO/CPAM were prepared on etched silicon wafers (the area of sample is 1 cm × 1 cm) for Atomic force microscopy (AFM) imaging conducted with a Bruker Multimode AFM system operating in the tapping mode. Nanosensor silicon probes (PPP-NCHR) were used with spring constants of 40 N/m and frequency of 78.6 kHz at 25 °C and 40% relative humidity. Fourier transform infrared (FT-IR) spectra were recorded with a Nicolet Avatar 360 spectrometer. The CPAM adsorption films were characterized using IR reflectance spectroscopy, and compared to CPAM tested by IR absorption spectroscopy using KBr pellets. Raman spectra were recorded from 800 to 3200 cm^{-1} on a JY HR800 using a laser wavelength at 633 nm.

All experiments for in situ monitoring of the adsorption behavior were carried out using a CHI430A electrochemical workstation equipped with a quartz crystal oscillator. The crystal coated with a disk-shaped gold film (diameter = 5.0 mm) was used as the working electrode, a Pt wire as the counter electrode and an $Hg/HgCl_2$ electrode as the reference electrode. The parameters for the quartz crystal microbalance were set as follows: f_0 = 7.995 MHz (resonant frequency of the quartz crystal) and A = 0.196 cm^2 (working area of the quartz crystal). A frequency decrease of 1.0 Hz was found to correspond to 1.34 ng of mass adsorbed on the crystal electrode surface.

Electrical resistance of the self-assembled film was measured by a four probe method (RTS-4, China) using a constant voltage of 10 V. The resistance value of each sample was calculated by averaging results from four tests.

3. RESULTS AND DISCUSSION

Excellent dispersion of GO in solution is essential to achieve uniform self-assembly. On the basis of early investigations to elucidate the specific atomic structures of GO,[40−43] the widely accepted structure consists of basal plane carbon atoms decorated with hydroxyl and epoxy functional groups,[44,45] which render GO nanosheets easily dispersible in aqueous solutions. Since the colloidal stability of a GO dispersion is strongly dependent on pH,[46] the effect of pH value on GO dispersions in aqueous solution was studied. As shown in Figure 1a, when the pH is 1.0, GO dispersion exhibits a pale yellow color. With rising pH levels, the GO dispersion gradually turns darker, appearing almost opaque at pH 12. When the solution appears a darker color, it can be inferred that a better dispersion of GO nanosheets has been achieved. Herein, the pH is adjusted to a value greater than 7.0 to achieve a stable dispersion of GO nanosheets, with an optimal pH value being in the range of 10 to 12, where the solution appears dark brown. The ζ potential, which represents the degree of

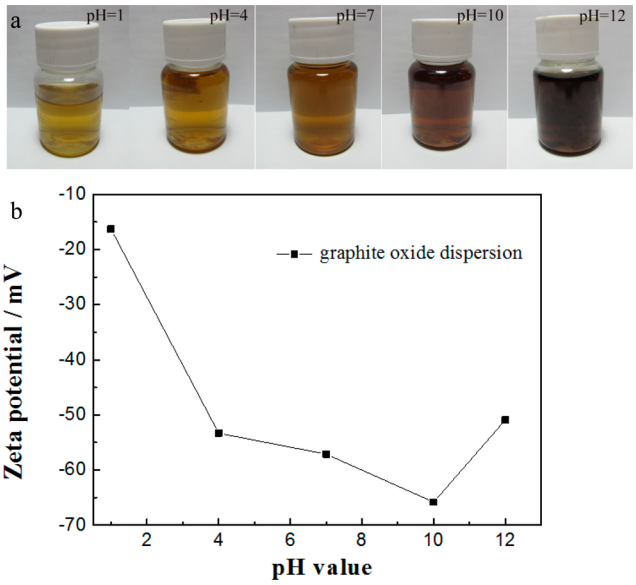

Figure 1. (a) Image of GO dispersion solution at different pH values, (b) pH values versus ζ potential for GO dispersion solution.

electrostatic repulsion between particles, is directly related to the colloidal dispersion stability. When the absolute value of ζ potential is higher, this indicates a more stable dispersion system where the colloidal particles are dissolved or dispersed in a solution with higher resistance to aggregation. As shown in Figure 1b, the ζ potential of the GO dispersion shifts toward a more negative voltage with increasing pH values. However, excessively alkaline conditions (pH = 12) lead to an increase of the ζ potential, which by extension influences the stability of the dispersed system. Therefore, an optimal pH value of 10.0 was determined to achieve well-dispersed GO nanosheets with the most negative surface charge (ζ potential, −68 mV) that would be more favorable for electrostatic attraction with the positively charged pretreatment layer during the self-assembly process.

CPAM is a water-soluble linear high polymer, synthesized by free radical polymerization of acrylamide (AM) and the cationic monomer. It has been determined that CPAM can be adsorbed on the surface of the epoxy resin by surface wetting.[47] As the pretreatment layer, the adsorption of CPAM was investigated on various surfaces. The changes of contact angle between a water drop and the various substrates (glass slides, epoxy plastic plates, and copper sheets) with CPAM pretreatment were measured as shown in Figure 2. The initial contact angle on the glass slide is slightly smaller (54°) than that of the epoxy and the copper sheet (approximately 70°), which exhibits more hydrophobicity. After soaking with the CPAM solution, the contact angle of the glass slide, epoxy plate and copper sheet decrease to 30°, 36°, and 43°, respectively. It is clear that CPAM can effectively adsorb on the surface of the various substrates, with the hydrophilic amino groups of the CPAM molecules facilitating the spreading of a water droplet on the various surfaces, resulting in a significant decrease of the contact angle.

To confirm the above prediction, the infrared reflection of the substrate after CPAM pretreatment was investigated as shown in Figure 2g. The absorption peak at 3430 cm^{-1} is attributed to $-NH_2-$ stretching. The band centered at 3196 cm^{-1} can be assigned to association N−H bending. The sharp

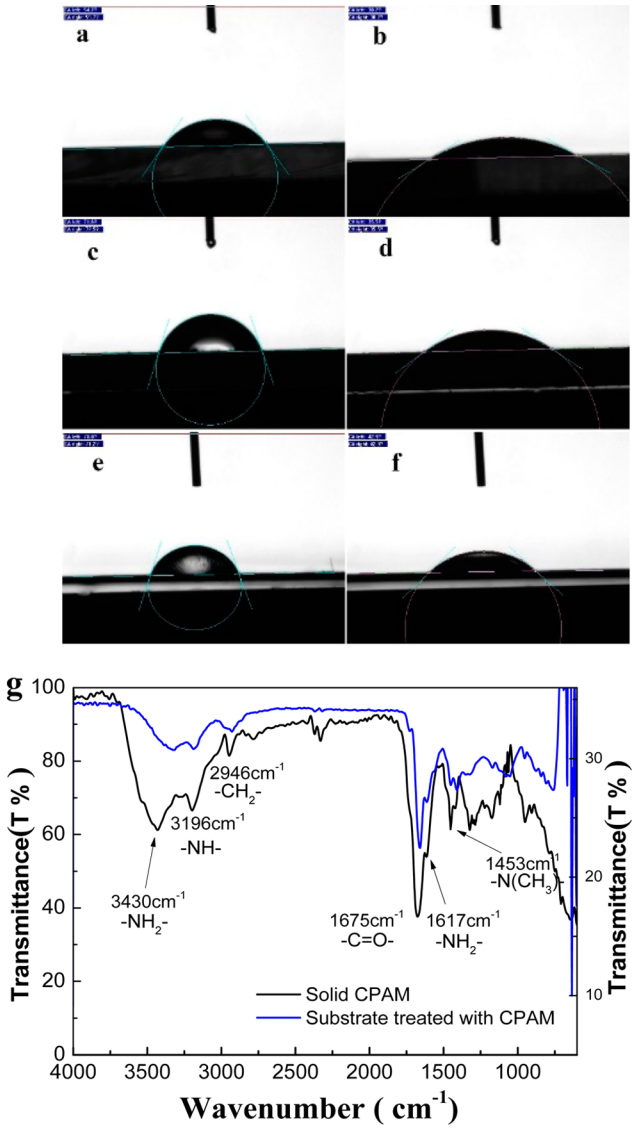

Figure 2. Contact angle measurements of a water droplet on (a) a glass slide substrate, (b) the glass slide after CPAM treatment, (c) an epoxy plastic plate substrate, (d) the epoxy plastic plate after the CPAM treatment, (e) a copper sheet substrate and (f) the copper sheet after the CPAM treatment. (g) FTIR spectra of the copper sheet treated with the CPAM solution, compared with solid CPAM.

peak at 2946 cm^{-1} is the result of asymmetric stretching vibration of $-CH_2-$, and the peaks at 1675 and 1617 cm^{-1} belong to the amide I (C═O stretching) and the amide II ($-NH_2$ bending), respectively.[48,49] The peak at 1453 cm^{-1} highlights the $-CH_3$ deformation vibration of -N(CH_3), indicating that the N−H group of the polyacrylamide has been replaced by N-R.[50,51] Meanwhile 950 cm^{-1} represents the existence of quaternary ammonium group. The spectral shape of the absorption of the CPAM pretreated sample generally coincides with that of solid CPAM, confirming that a CPAM coating remains on the substrate surface after rinsing.

Pretreatment solutions with different CPAM concentrations (1, 5, 10 mg/L) were added into the electrolytic cell of an EQCM to investigate the adsorption behavior on the substrate. The correlations between frequency and time are shown in Figure 3. DI water, used as a blank sample, shows negligible changes in oscillator frequency, reflecting no adsorption−

dx.doi.org/10.1021/am504941p | ACS Appl. Mater. Interfaces 2014, 6, 19783−19790

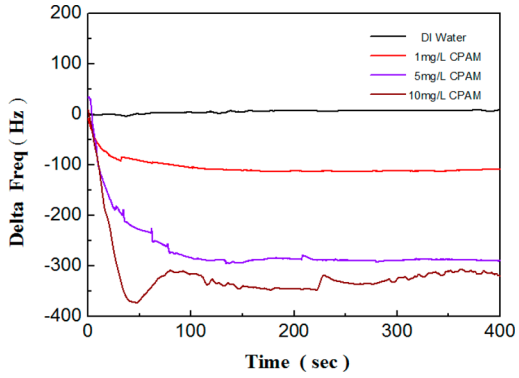

Figure 3. Oscillation frequency of the Au covered quartz electrode as a function of CPAM concentrations.

desorption reactions occurring at the electrode interface as expected. However, the frequency shifts to more negative values when using CPAM containing solutions, indicating the deposition of CPAM on the electrode surface. In comparison with DI water, a decrease of nearly 100 Hz in the frequency is observed with a CPAM concentration of 1 mg/L. When the CPAM concentration is increased up to 5 mg/L, the frequency curve significantly drops to −300 Hz. Only a slight decrease in frequency is observed with further increasing the CPAM concentration to 10 mg/L. Thus, it is apparent that with increasing CPAM concentration, the adsorbed amount will rise in a nonlinear fashion. Additionally, it is observed that all the adsorption equilibrium is established within 150s. The CPAM layers are created by the adsorption of CPAM on the substrate surface from the aqueous solution.[52] It is proposed that the assembled CPAM at the interface might capture CPAM molecules dissolved in the solution by the affinity adsorption of molecular chain, thereby resulting in continuous thickening of the adsorption layer until the adsorption equilibrium has been reached. Accordingly, increasing CPAM concentrations will raise the likelihood of this occurrence.

To pursue driving force during self-assembly which have rarely been reported, electrostatic interactions between GO and CPAM were investigated using different polarization potentials in EQCM. The applied polarization is shown in Figure 4 as a dashed line. First, the voltage is maintained at open circuit potential for 200s and then at an anodic polarization of 0.2 V (vs open circuit potential) for 200s, repeating the cycle once

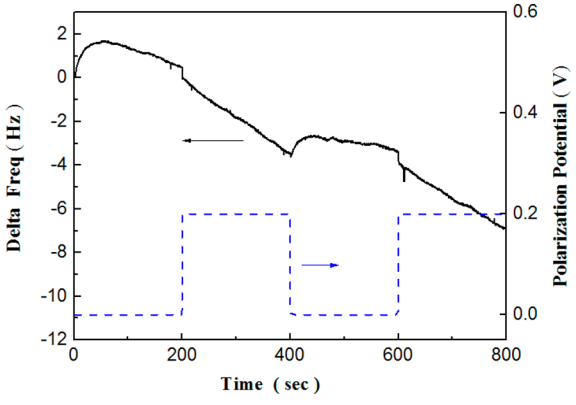

Figure 4. Corresponding oscillation frequency variations of GO nanosheets with different polarizations on the Au covered quartz electrode.

again. In the beginning small bubbles possibly moved away from the electrode surface by oscillating shock, resulting in the slight rise in frequency. When the working electrode was polarized, the frequency declined rapidly, indicating that the negatively charged GO was binding to the electrode surface through Coulombic forces. After one cycle (at 400 s) and restoration of open circuit potential, the ascent of the frequency again is attributed to the partial desorption of GO nanosheets. Upon polarizing to 0.2 V again, the frequency resumed its decline, indicating further adsorption of GO. The interactions between CPAM and GO were further investigated by the following experiments. Figure 5a displays a photo of a well-

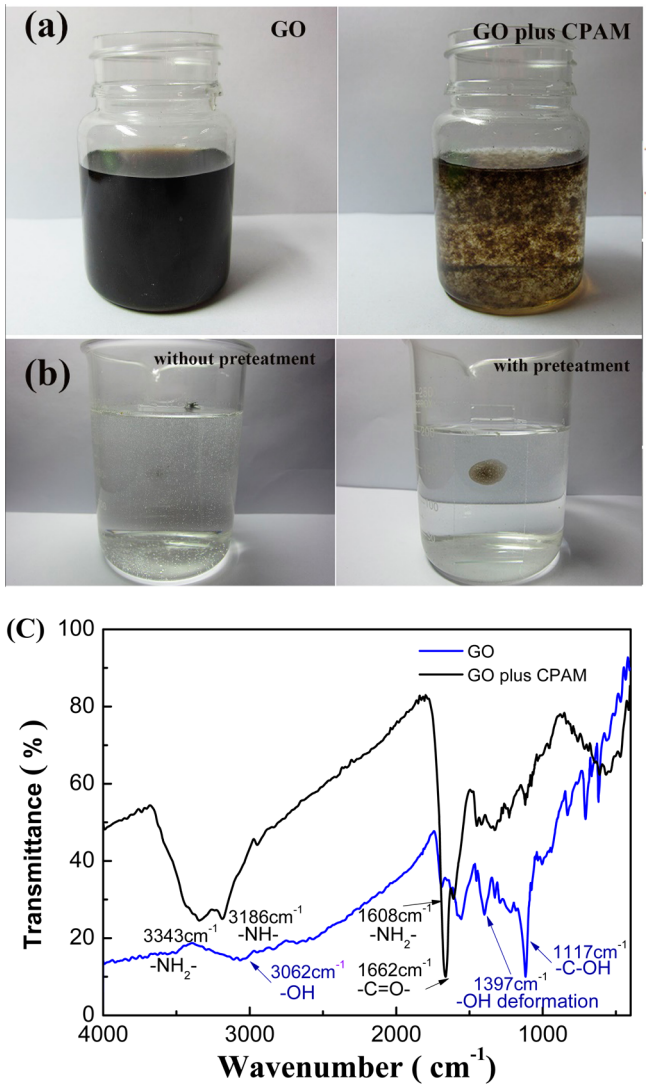

Figure 5. (a) Image of GO dispersion before and after the addition of CPAM, (b) influence of pretreatment on the self-assembled GO layers in sodium borohydride, and (c) FTIR spectra of GO (solid blue line) and the mixture of GO and CPAM (solid black line) using KBr pellets.

dispersed GO nanosheets (0.1 mg/mL, 50 mL) at pH 10.0. After adding 2 mL of 10 mg/L CPAM and allowing it to stir for 10 min, the color of the solution turned to a lighter brown, indicating aggregation of the GO particles due to the flocculation behavior of CPAM. This observation suggests that CPAM possesses the desirable surface properties to provide adhesion as a pretreatment layer for the self-assembly

of GO nanosheets. To explore the stability of the composite film during rapid chemical reduction, glass slides with CPAM pretreatment covered GO films, as compared to that without pretreatment, were immersed in sodium borohydride solution for 1 h. As shown in Figure 5(b), for the glass slide without pretreatment the whole GO film detached from the substrate and suspended in the liquid solution owing to the poor binding with the substrate. On the contrary, the GO film on the glass slide pretreated with CPAM remained intact under the impact of bubbles during the reduction, verifying that the CPAM pretreatment layer strengthen the binding between the GO film and the substrate.

Infrared spectra of the GO and GO/CPAM samples are shown in Figure 5c. The spectra of the GO sample show a broad band centered at 3062 cm^{-1} which is attributed to the O−H stretching vibration of GO. The typical absorption peak near 1117 cm^{-1} is the result of the C−OH stretching vibration. The peak at 1397 cm^{-1} is assigned to O−H deformations of C−O−H groups, whereby GO's high solubility in water is due to the presence of these hydroxyl groups. In addition, the absorption peak at 1218 cm^{-1} belongs to the C−O−C stretching vibration. The peak at 1688 cm^{-1} corresponds to the C═O stretching vibration, indicating the presence of the carboxyl functional group which also contributes to the high solubility of GO in water. The IR spectrum of a mixture of GO and CPAM, after drying to remove moisture, presents the main characteristic peaks of solid CPAM. In particular, it is worth noting that the absorption peaks at 3443 and 3196 cm^{-1} attributed to N−H stretching transfer to 3343 and 3186 cm^{-1}, respectively, while those at 1675 and 1617 cm^{-1} relating to the amide species shift to 1662 and 1608 cm^{-1}. The reason for adsorption peaks shift to lower wave numbers is the result of the influence of the intermolecular hydrogen bonds produced between the amino groups of CPAM and the hydroxyl groups of GO. Moreover, there are no new absorption peaks arising from the combination process, implying no chemical reaction occurred.

According to our analysis presented above, a proposed schematic of self-assembly of GO nanosheets on the CPAM layer is shown in Figure 6. It is considered that self-assembly can be divided into two major processes. First, GO nanosheets, which possess oxygen-containing functional groups with negative charges, are attracted to the surface of the CPAM layer because of the electrostatic force. Second, the lamellar GO nanosheets tends to deposit on the substrate surface and are wrapped by the long multibranched carbon chains of the CPAM molecules. In addition, the hydrogen bonds discussed previously further strengthen this combination.

A SEM image of the GO/CPAM composite film is shown in Figure 7a. It can be seen that the assembled GO layer is extremely smooth and flat. Only some microscopic ripples of the GO layer was illustrated by AFM in Figure 7b. A height variation of approximately 5 nm, quite distinct from the atomically rough surface of GO nanosheets,[53] may result from nonuniform deposition of the CPAM pretreatment layer or assembled GO nanosheets.

When a glass slide treated with CPAM was immersed directly into a GO (0.1 mg/mL) solution for 10 min, followed by rinsing with DI water and drying, a nearly transparent and uniform GO/CPAM film appears on the entire slide surface as shown in Figure 8a. With the reduction in a sodium borohydride solution at room temperature, the color of the film became darker, while bubbles simultaneously was

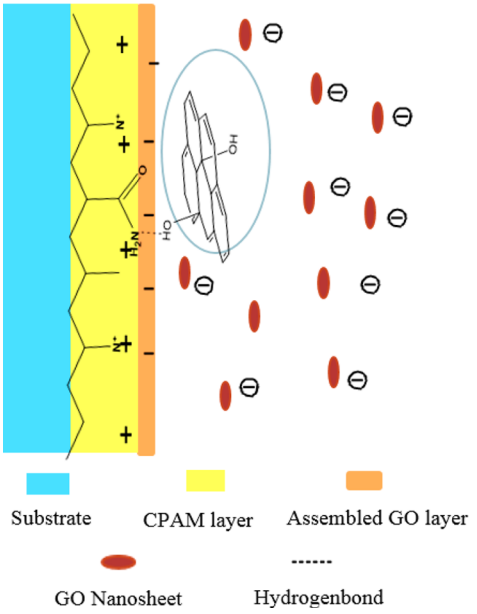

Figure 6. Proposed schematic of GO nanosheets assembled on the CPAM layer.

generated in the solution. The end result was a gray conductive film obtained on the surface of the glass slide (Figure 8b), indicating that the assembled GO layer was successfully reduced.

The reduction effect of the composite film in sodium borohydride was investigated by Raman spectra and electrical measurements. Figure 8c shows the Raman spectra of pure graphite, CPAM film, GO/CPAM composite film, and R-GO/CPAM composite film. It is apparent that underlying CPAM layer shows no obvious Raman scattering peak that will not affect the results of the self-assembled GO layer. As the graphene-based materials, the significant D band (1350 cm^{-1}) is observed, representing defect species, along with the G band (1588 cm^{-1}) produced by stretching of sp^2 carbon atoms. The integrated intensity ratio of the I_D/I_G peak can be used to describe the defect degree and grain sizes of the carbon crystal structure.[54] Pure flake graphite as a comparison displays a sharp G peak as expected, while the D peak is relatively insignificant. For GO/CPAM composite film, the D and G bands are also broadened, and the D band peak becomes prominent with an I_D/I_G ratio of 1.22, indicating the fracture of the integrated graphite structural order under the intense oxidation. After sodium borohydride reduction, the higher I_D/I_G ratio (1.49) of R-GO/CPAM composite film is contrary to the recovery of the graphite crystal structure through removal of oxygen species and ascribable to the reduced average crystallite size of the sp^2 bonded carbons in accordance with previously reported Raman spectra of R-GO.[2,27] The substrate and the adsorbed CPAM as the pretreatment layer exhibit electrical insulation. Just the self-assembled GO layer became conductive after chemical reduction. At the same time, the surface resistance of the self-assembled films gradually decreased with variation of time, with results shown in Figure 8d. It is expected the sheet resistances of the films are consistent with the degree of reduction. No measurable resistances are observed (exceeding 20 MΩ/sq) in first few minutes during reduction, and after 10 min, the resistance value decreased to 53.7 kΩ/sq, indicating a significant increase in the degree of reduction. A stable

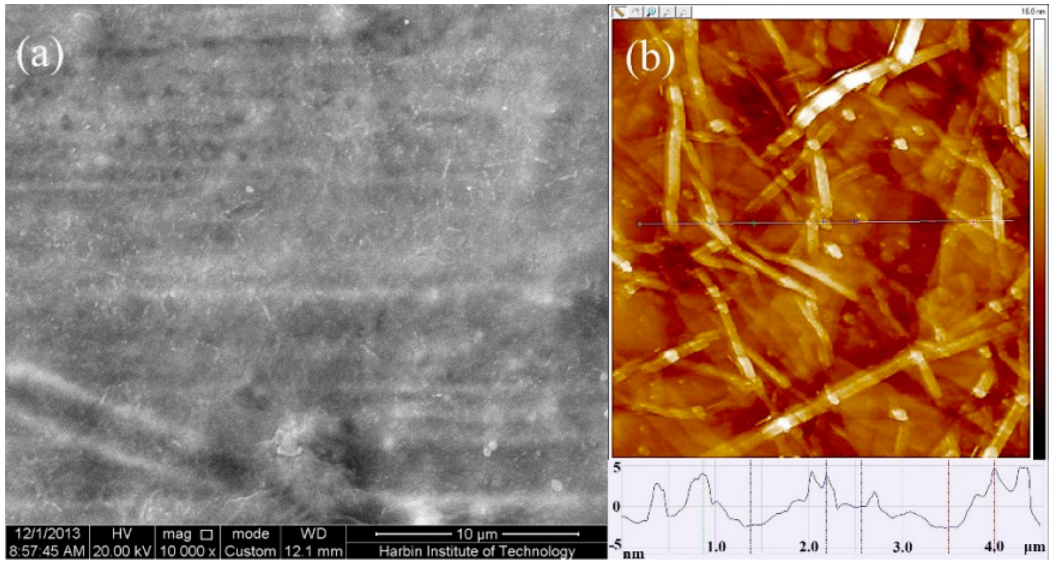

Figure 7. (a) SEM image of GO/CPAM composite film and (b) AFM image of GO/CPAM composite film on the silicon wafer.

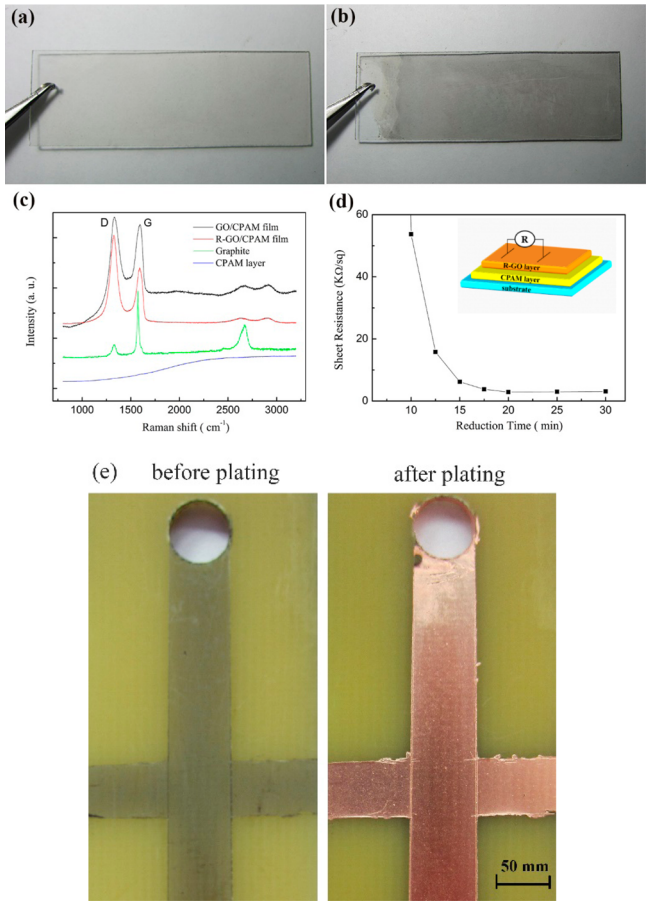

Figure 8. (a) Self-assembled GO/CPAM composite film, (b) R-GO/CPAM composite film on glass slides after reduction, (c) Raman spectrum of pure graphite, CPAM film, GO/CPAM composite film and R-GO/CPAM composite film, (d) the resistance of R-GO/CPAM composite film variations with reduction time, and (e) copper plating on the self-assembled R-GO/CPAM film.

resistance (3.1 kΩ/sq) is achieved at 20 min, displaying no further changes with an increase of time. This resistance value is also in close agreement with a value reported previously for R-GO.[22] It is therefore demonstrated that the assembled GO film has been completely reduced in the sodium borohydride solution. Drawing on the fact that conductive R-GO/CPAM thin films can be prepared on a variety of substrates, a patterned conductive film was formed by self-assembly on a printed circuit board as shown in Figure 8e. One end of the board was connected to a cathode lead for plating under a constant current of 20 mA in an acid copper plating solution. A continuous copper layer covering the patterned film was achieved after 30 min. Clearly, the R-GO/CPAM composite film as a conductive layer enabled the electrodeposition of copper onto nonconductive substrates. This direct, patterned electroplating on the surface of circuit boards demonstrates the application potential of R-GO/CPAM composite films in the field of electronics.

4. CONCLUSION

In this work, a GO/CPAM composite film was prepared by a unique self-assembly process in an aqueous solution, followed by rapid room temperature reduction in sodium borohydride solution, resulting in substrate-supported electrically conductive thin films. During the preparation stage, aqueous GO solution was initially optimized to be pH 10, corresponding to the maximum ζ potential of −68 mV that would be favorable for self-assembly process. Then nonconductive substrate was coated by CPAM, forming a hydrophobic layer that was used to facilitate the self-assembly of GO. Importantly, the self-assembly process of CPAM and GO was systematically investigated by the quartz crystal microbalance technique, revealing the adsorption properties of CPAM and electrostatic forces between CPAM and GO. In addition, the intermolecular hydrogen bonds produced between the amino groups of CPAM and the hydroxyl groups of GO were determined by IR spectroscopy. Raman spectra and surface resistance value confirmed that the assembled GO film has been fully reduced in the sodium borohydride solution. To our knowledge, this is the first time sodium borohydride, considered to have low toxicity, is used for the in situ reduction of a self-assembled GO film. In summary, it provides a highly effective, simplistic and timely method to prepare self-assembled R-GO films. Among various potential applications, it is demonstrated the possibility

to prepare a copper coating on conductive patterned R-GO/CPAM films on the surface of circuit boards by direct electroplating.

AUTHOR INFORMATION

Corresponding Authors

*E-mail: ninglihit@263.net.

*E-mail: gangwu@buffalo.edu.

Notes

The authors declare no competing financial interest.

ACKNOWLEDGMENTS

G.W.'s Startup fund from the University at Buffalo (SUNY) and Los Alamos National Laboratory LDRD Program financially supported this work and are gratefully acknowledged.

REFERENCES

(1) Novoselov, K. S.; Geim, A. K.; Morozov, S. V.; Jiang, D.; Zhang, Y.; Dubonos, S. V.; Grigorieva, I. V.; Firsov, A. A. Electric Field Effect in Atomically Thin Carbon Films. *Science* **2004**, *306*, 666−669.

(2) Stankovich, S.; Dikin, D. A.; Piner, R. D.; Kohlhaas, K. A.; Kleinhammes, A.; Jia, Y.; Wu, Y.; Nguyen, S. T.; Ruoff, R. S. Synthesis of Graphene-Based Nanosheets Via Chemical Reduction of Exfoliated Graphite Oxide. *Carbon* **2007**, *45*, 1558−1565.

(3) Novoselov, K. S.; Jiang, Z.; Zhang, Y.; Morozov, S.; Stormer, H.; Zeitler, U.; Maan, J.; Boebinger, G.; Kim, P.; Geim, A. Room-Temperature Quantum Hall Effect in Graphene. *Science* **2007**, *315*, 1379−1379.

(4) Orlita, M.; Faugeras, C.; Plochocka, P.; Neugebauer, P.; Martinez, G.; Maude, D. K.; Barra, A. L.; Sprinkle, M.; Berger, C.; de Heer, W. A.; Potemski, M. Approaching the Dirac Point in High-Mobility Multilayer Epitaxial Graphene. *Phys. Rev. Lett.* **2008**, *101*, No. 267601.

(5) Kim, K. S.; Zhao, Y.; Jang, H.; Lee, S. Y.; Kim, J. M.; Ahn, J. H.; Kim, P.; Choi, J. Y.; Hong, B. H. Large-Scale Pattern Growth of Graphene Films for Stretchable Transparent Electrodes. *Nature* **2009**, *457*, 706−710.

(6) Wang, Y.; Sun, H.; Zhang, R.; Yu, S. N.; Kong, J. L. Large Scale Templated Synthesis of Single-Layered Graphene with a High Electrical Capacitance. *Carbon* **2013**, *53*, 245−251.

(7) Hernandez, Y.; Nicolosi, V.; Lotya, M.; Blighe, F. M.; Sun, Z.; De, S.; McGovern, I.; Holland, B.; Byrne, M.; Gun'Ko, Y. K. High-Yield Production of Graphene by Liquid-Phase Exfoliation of Graphite. *Nat. Nanotechnol.* **2008**, *3*, 563−568.

(8) Lv, Z.; Yang, X.; Wang, E. Highly Concentrated Polycations-Functionalized Graphene Nanosheets with Excellent Solubility and Stability, and Its Fast, Facile and Controllable Assembly of Multiple Nanoparticles. *Nanoscale* **2013**, *5*, 663−670.

(9) Jeon, I.-Y.; Choi, H.-J.; Jung, S.-M.; Seo, J.-M.; Kim, M.-J.; Dai, L.; Baek, J.-B. Large-Scale Production of Edge-Selectively Functionalized Graphene Nanoplatelets Via Ball Milling and Their Use as Metal-Free Electrocatalysts for Oxygen Reduction Reaction. *J. Am. Chem. Soc.* **2013**, *135*, 1386−1393.

(10) Berger, C.; Song, Z.; Li, X.; Wu, X.; Brown, N.; Naud, C.; Mayou, D.; Li, T.; Hass, J.; Marchenkov, A. N.; Conrad, E. H.; First, P. N.; de Heer, W. A. Electronic Confinement and Coherence in Patterned Epitaxial Graphene. *Science* **2006**, *312*, 1191−1196.

(11) Sutter, P. W.; Flege, J. I.; Sutter, E. A. Epitaxial Graphene on Ruthenium. *Nat. Mater.* **2008**, *7*, 406−411.

(12) Wintterlin, J.; Bocquet, M. L. Graphene on Metal Surfaces. *Surf. Sci.* **2009**, *603*, 1841−1852.

(13) Iwasaki, T.; Park, H. J.; Konuma, M.; Lee, D. S.; Smet, J. H.; Starke, U. Long-Range Ordered Single-Crystal Graphene on High-Quality Heteroepitaxial Ni Thin Films Grown on MgO(111). *Nano Lett.* **2010**, *11*, 79−84.

(14) Li, Q.; Xu, P.; Gao, W.; Ma, S.; Zhang, G.; Cao, R.; Cho, J.; Wang, H.-L.; Wu, G. Graphene/Graphene-Tube Nanocomposites Templated from Cage-Containing Metal-Organic Frameworks for Oxygen Reduction in Li−O_2 Batteries. *Adv. Mater.* **2014**, *26*, 1378−1386.

(15) Wu, G.; Mack, N. H.; Gao, W.; Ma, S.; Zhong, R.; Han, J.; Baldwin, J. K.; Zelenay, P. Nitrogen-Doped Graphene-Rich Catalysts Derived from Heteroatom Polymers for Oxygen Reduction in Nonaqueous Lithium−O_2 Battery Cathodes. *ACS Nano* **2012**, *6*, 9764−9776.

(16) Li, Q.; Cao, R.; Cho, J.; Wu, G. Nanocarbon Electrocatalysts for Oxygen Reduction in Alkaline Media for Advanced Energy Conversion and Storage. *Adv. Energy Mater.* **2014**, *4*, DOI: 10.1002/aenm.201301415.

(17) He, Q.; Li, Q.; Khene, S.; Ren, X.; López-Suárez, F. E.; Lozano-Castelló, D.; Bueno-López, A.; Wu, G. High-Loading Cobalt Oxide Coupled with Nitrogen-Doped Graphene for Oxygen Reduction in Anion-Exchange-Membrane Alkaline Fuel Cells. *J. Phys. Chem. C* **2013**, *117*, 8697−8707.

(18) Wang, J. C.; Zhou, T. N.; Deng, H.; Chen, F.; Wang, K.; Zhang, Q.; Fu, Q. An Environmentally Friendly and Fast Approach to Prepare Reduced Graphite Oxide with Water and Organic Solvents Solubility. *Colloids Surf., B* **2013**, *101*, 171−176.

(19) Pei, S.; Zhao, J.; Du, J.; Ren, W.; Cheng, H.-M. Direct Reduction of Graphene Oxide Films into Highly Conductive and Flexible Graphene Films by Hydrohalic Acids. *Carbon* **2010**, *48*, 4466−4474.

(20) Zhang, J.; Yang, H.; Shen, G.; Cheng, P.; Zhang, J.; Guo, S. Reduction of Graphene Oxide Via L-Ascorbic Acid. *Chem. Commun.* **2010**, *46*, 1112−1114.

(21) Li, X.; Zhang, G.; Bai, X.; Sun, X.; Wang, X.; Wang, E.; Dai, H. Highly Conducting Graphene Sheets and Langmuir−Blodgett Films. *Nat. Nanotechnol.* **2008**, *3*, 538−542.

(22) Zhao, J.; Pei, S.; Ren, W.; Gao, L.; Cheng, H. M. Efficient Preparation of Large-Area Graphene Oxide Sheets for Transparent Conductive Films. *ACS Nano* **2010**, *4*, 5245−5252.

(23) Park, K. H.; Kim, B. H.; Song, S. H.; Kwon, J.; Kong, B. S.; Kang, K.; Jeon, S. Exfoliation of Non-Oxidized Graphene Flakes for Scalable Conductive Film. *Nano Lett.* **2012**, *12*, 2871−2876.

(24) Gao, W.; Wu, G.; Janicke, M. T.; Cullen, D. A.; Mukundan, R.; Baldwin, J. K.; Brosha, E. L.; Galande, C.; Ajayan, P. M.; More, K. L.; Dattelbaum, A. M.; Zelenay, P. Ozonated Graphene Oxide Film as a Proton-Exchange Membrane. *Angew. Chem., Int. Ed.* **2014**, *53*, 3588−3593.

(25) Wang, X.; Zhi, L.; Müllen, K. Transparent, Conductive Graphene Electrodes for Dye-Sensitized Solar Cells. *Nano Lett.* **2007**, *8*, 323−327.

(26) Eda, G.; Fanchini, G.; Chhowalla, M. Large-Area Ultrathin Films of Reduced Graphene Oxide as a Transparent and Flexible Electronic Material. *Nat. Nanotechnol.* **2008**, *3*, 270−274.

(27) Shin, H.-J.; Kim, K. K.; Benayad, A.; Yoon, S.-M.; Park, H. K.; Jung, I.-S.; Jin, M. H.; Jeong, H.-K.; Kim, J. M.; Choi, J.-Y.; Lee, Y. H. Efficient Reduction of Graphite Oxide by Sodium Borohydride and Its Effect on Electrical Conductance. *Adv. Funct. Mater.* **2009**, *19*, 1987−1992.

(28) Xia, G.; Li, N.; Li, D.; Liu, R.; Wang, C.; Li, Q.; Lü, X.; Spendelow, J. S.; Zhang, J.; Wu, G. Graphene/Fe_2O_3/SnO_2 Ternary Nanocomposites as a High-Performance Anode for Lithium Ion Batteries. *ACS Appl. Mater. Interfaces* **2013**, *5*, 8607−8614.

(29) Stankovich, S.; Dikin, D. A.; Dommett, G. H.; Kohlhaas, K. M.; Zimney, E. J.; Stach, E. A.; Piner, R. D.; Nguyen, S. T.; Ruoff, R. S. Graphene-Based Composite Materials. *Nature* **2006**, *442*, 282−286.

(30) Tien, H. W.; Huang, Y. L.; Yang, S. Y.; Hsiao, S. T.; Liao, W. H.; Li, H. M.; Wang, Y. S.; Wang, J. Y.; Ma, C. C. M. Preparation of Transparent, Conductive Films by Graphene Nanosheet Deposition on Hydrophilic or Hydrophobic Surfaces through Control of the pH Value. *J. Mater. Chem.* **2012**, *22*, 2545−2552.

(31) Bourdo, S. E.; Viswanathan, T. Graphite/Polyaniline (GP) Composites: Synthesis and Characterization. *Carbon* **2005**, *43*, 2983−2988.

(32) Trang, L. K. H.; Tung, T. T.; Kim, T. Y.; Yang, W. S.; Kim, H.; Suh, K. S. Preparation and Characterization of Graphene Composites with Conducting Polymers. *Polym. Int.* **2012**, *61*, 93−98.

(33) Osterholm, A.; Lindfors, T.; Kauppila, J.; Damlin, P.; Kvarnstrom, C. Electrochemical Incorporation of Graphene Oxide into Conducting Polymer Films. *Electrochim. Acta* **2012**, *83*, 463−470.
(34) Wu, C.; Huang, X. Y.; Wang, G. L.; Lv, L. B.; Chen, G.; Li, G. Y.; Jiang, P. K. Highly Conductive Nanocomposites with Three-Dimensional, Compactly Interconnected Graphene Networks Via a Self-Assembly Process. *Adv. Funct. Mater.* **2013**, *23*, 506−513.
(35) Kotov, N. A.; Dékány, I.; Fendler, J. H. Ultrathin Graphite Oxide−Polyelectrolyte Composites Prepared by Self-Assembly: Transition between Conductive and Non-Conductive States. *Adv. Mater.* **1996**, *8*, 637−641.
(36) Kovtyukhova, N. I.; Ollivier, P. J.; Martin, B. R.; Mallouk, T. E.; Chizhik, S. A.; Buzaneva, E. V.; Gorchinskiy, A. D. Layer-by-Layer Assembly of Ultrathin Composite Films from Micron-Sized Graphite Oxide Sheets and Polycations. *Chem. Mater.* **1999**, *11*, 771−778.
(37) Szabó, T.; Szeri, A.; Dékány, I. Composite Graphitic Nanolayers Prepared by Self-Assembly between Finely Dispersed Graphite Oxide and a Cationic Polymer. *Carbon* **2005**, *43*, 87−94.
(38) Shi, Y.; Ju, B.; Zhang, S. Flocculation Behavior of a New Recyclable Flocculant Based on pH Responsive Tertiary Amine Starch Ether. *Carbohy. Poly.* **2012**, *88*, 132−138.
(39) Hummers, W. S., Jr.; Offeman, R. E. Preparation of Graphitic Oxide. *J. Am. Chem. Soc.* **1958**, *80*, 1339−1339.
(40) Kudin, K. N.; Ozbas, B.; Schniepp, H. C.; Prud'homme, R. K.; Aksay, I. A.; Car, R. Raman Spectra of Graphite Oxide and Functionalized Graphene Sheets. *Nano Lett.* **2007**, *8*, 36−41.
(41) Cai, W.; Piner, R. D.; Stadermann, F. J.; Park, S.; Shaibat, M. A.; Ishii, Y.; Yang, D.; Velamakanni, A.; An, S. J.; Stoller, M. Synthesis and Solid-State NMR Structural Characterization of ^{13}C-Labeled Graphite Oxide. *Science* **2008**, *321*, 1815−1817.
(42) Mkhoyan, K. A.; Contryman, A. W.; Silcox, J.; Stewart, D. A.; Eda, G.; Mattevi, C.; Miller, S.; Chhowalla, M. Atomic and Electronic Structure of Graphene-Oxide. *Nano Lett.* **2009**, *9*, 1058−1063.
(43) Gómez-Navarro, C.; Meyer, J. C.; Sundaram, R. S.; Chuvilin, A.; Kurasch, S.; Burghard, M.; Kern, K.; Kaiser, U. Atomic Structure of Reduced Graphene Oxide. *Nano Lett.* **2010**, *10*, 1144−1148.
(44) *Structure of Graphite Oxide Revisited*, No. 102; American Chemical Society: Washington, DC, 1998.
(45) He, H.; Klinowski, J.; Forster, M.; Lerf, A. A New Structural Model for Graphite Oxide. *Chem. Phys. Lett.* **1998**, *287*, 53−56.
(46) Li, D.; Muller, M. B.; Gilje, S.; Kaner, R. B.; Wallace, G. G. Processable Aqueous Dispersions of Graphene Nanosheets. *Nat. Nanotechnol.* **2008**, *3*, 101−105.
(47) Angelopoulos, A. P.; Benziger, J. B.; Wesson, S. P. Cationic Polyacrylamide Adsorption on Epoxy Surfaces. *J. Colloid Interface Sci.* **1997**, *185*, 147−156.
(48) Chiem, L. T.; Huynh, L.; Ralston, J.; Beattie, D. A. An in Situ ATR−FTIR Study of Polyacrylamide Adsorption at the Talc Surface. *J. Colloid Interface Sci.* **2006**, *297*, 54−61.
(49) Tang, Q. W.; Lin, J. M.; Wu, J. H. The Preparation and Electrical Conductivity of Polyacrylamide/Graphite Conducting Hydrogel. *J. Appl. Polym. Sci.* **2008**, *108*, 1490−1495.
(50) Wang, L.-J.; Wang, J.-P.; Zhang, S.-J.; Chen, Y.-Z.; Yuan, S.-J.; Sheng, G.-P.; Yu, H.-Q. A Water-Soluble Cationic Flocculant Synthesized by Dispersion Polymerization in Aqueous Salts Solution. *Sep. Purif. Technol.* **2009**, *67*, 331−335.
(51) Zhu, J.; Zhang, G.; Li, J. Preparation of Amphoteric Polyacrylamide Flocculant and Its Application in the Treatment of Tannery Wastewater. *J. Appl. Polym. Sci.* **2011**, *120*, 518−523.
(52) Munro, J. C.; Frank, C. W. Polyacrylamide Adsorption from Aqueous Solutions on Gold and Silver Surfaces Monitored by the Quartz Crystal Microbalance. *Macromolecules* **2004**, *37*, 925−938.
(53) Stolyarova, E.; Rim, K. T.; Ryu, S.; Maultzsch, J.; Kim, P.; Brus, L. E.; Heinz, T. F.; Hybertsen, M. S.; Flynn, G. W. High-Resolution Scanning Tunneling Microscopy Imaging of Mesoscopic Graphene Sheets on an Insulating Surface. *Pro. Nat. Acad. Sci.* **2007**, *104*, 9209−9212.
(54) Das, A.; Chakraborty, B.; Sood, A. K. Raman Spectroscopy of Graphene on Different Substrates and Influence of Defects. *Bull. Mater. Sci.* **2008**, *31*, 579−584.